LIMNOLOGY
and
OCEANOGRAPHY

ASLO

Limnol. Oceanogr. 66, 2021, 1475–1491

doi: 10.1002/lno.11698

Seasonality and biological forcing modify the diel frequency of nearshore pH extremes in a subarctic Alaskan estuary

Cale A. Miller [1]*, **Amanda L. Kelley** [2]

[1]Department of Evolution and Ecology, University of California Davis, Davis, California
[2]College of Fisheries and Ocean Sciences, University of Alaska Fairbanks, Fairbanks, Alaska

Abstract

Acidification in nearshore waters is influenced by a multitude of drivers that shape the dynamics of pH and carbonate chemistry variability on diurnal, seasonal, and yearly time scales. Monitoring efforts aimed at characterizing high temporal variability are lacking in many nearshore systems, particularly in high-latitude regions such as Alaska. To rectify this, a nearshore acidification sensor array was established in the Fall of 2017 within Kachemak Bay, Alaska. Presented here are the results from the first year of these deployments, and the first record of a year-long high-frequency pH time series for nearshore Alaska. SeaFET™ pH and O_2 sensors deployed in Jakolof Bay and Bear Cove reveal a seasonally dynamic system in which nearshore waters in these two enclosed bays transition to being predominantly net autotrophic systems for a period of 60-plus days. High rates and durations of primary production in late spring and early summer create high pH conditions and extreme variability. Observed pH values in Jakolof Bay and Bear Cove tracked hourly rates of change on the order of 0.18 and 0.10 units, respectively. In Jakolof Bay nondirectional variability within a 12-h period was > 1 pH unit, exposing organisms to unstable, nonstatic pH conditions on tidal and diurnal cycles. Consistent frequency patterns detailing the magnitude of pH variability was correlated to tidal and O_2 signatures, elucidating the dynamics and drivers of pH variability. This first year of observations is the first step in quantifying the anthropogenic contribution to acidification for Kachemak Bay in the forthcoming years.

The global phenomenon of ocean acidification has resulted in a reduction in the ocean's buffering capacity as the hydrolysis of absorbed atmospheric CO_2 increases dissolved inorganic carbon, lowering carbonate ion concentration and seawater pH. In response to this ocean change, interconnected regional networks have been established to monitor and report the chemical changes occurring within the carbonate system (Mathis and Feely 2013; Newton et al. 2015). The purpose of this global ocean acidification network (http://goa-on.org) is to observe how acidification affects ecosystems from the tropics to the arctic within the context of marine resource viability. Specific to the United States, Alaskan aquaculture and fisheries are highly vulnerable to the effects of acidification due to a higher degree of social and economic reliance on marine resources (Ekstrom et al. 2015; Mathis et al. 2015*a*). A recent meta-analysis has shown that marine species in Alaska's polar regions are particularly sensitive to acidification (Kelley and Lunden 2017). And from a geochemical perspective, Alaskan coastal waters are more susceptible to acidification due to the intrinsic ability of these cold, high-latitude waters, to hold more TCO_2 due to enhanced CO_2 solubility and the equilibrium effects of colder water on carbonate chemistry thermodynamics (Fabry et al. 2009). In addition, nearshore Alaskan habitats are highly productive in the boreal spring and summer. The resulting organic carbon remineralization from the demise of this new production and increased freshwater input markedly increases TCO_2 leading to seasonal acidification events (Fabry et al. 2009; Mathis et al. 2015*b*; Siedlecki et al. 2017). Tracking acidification events and temporal trends in Alaskan coastal waters has taken a multifaceted approach: moored PCO_2 sensors and ship-based bottle sampling of TCO_2 and total alkalinity (TA) in deep waters (Gulf of Alaska and Bering sea), shore-based continuous PCO_2 sampling by Burke-o-Lators (Hales et al. 2004; Bandstra et al. 2006) on southeast and central coasts, nearshore pH monitoring with autonomous sensors within Cook Inlet's Kachemak Bay (this study), and Saildrones in Southcentral Prince William Sound (Dugan et al. 2017). While this effort has seen robust traction in the past few years,

*Correspondence: cmill@ucdavis.edu

Additional Supporting Information may be found in the online version of this article.

high spatial and temporal resolution measurements are still lagging in areas such as Kachemak Bay, where tidal prisms are extreme and biodiversity rich.

Kachemak Bay is located in the northern part of the Gulf of Alaska within Cook Inlet and has one of the largest tidal ranges in the world at ~ 8 m. The major freshwater inputs into the bay include the Fox River delta at the head, and seven glacial streams that are predominantly in the head-ward, northern part of the bay (Alaska Department of Fish and Game 1998; Schoch and Chenelot 2004). Tidal flushing along with riverine and glacial meltwater flux into the bay are physical processes that contribute to acidification variability (Evans et al. 2014; Waldbusser and Salisbury 2014; Beckwith et al. 2019). Homer Spit spatially separates the bay into inner and outer basins. The inner basin receives the bulk of glacial silt and freshwater discharge as well as riverine freshwater, and the outer basin is more oceanic influenced aside from a few glacial streams along the southeastern shore (Alaska Department of Fish and Game 1998; Schoch and Chenelot 2004). Surface waters in the outer basin can be affected by CO_2 rich, upwelled water, from the Gulf of Alaska entering through Cook Inlet, while the inner basin is a partially mixed estuary where precipitation and freshwater runoff exceed evaporation (Trasky et al. 1977; Alaska Department of Fish and Game 1998).

The complex geomorphology and oceanography of this region make Kachemak Bay one of the most biodiverse and biologically productive bays in subarctic waters (Alaska Department of Fish and Game 2001). Protected coves provide habitat for annual dense macroalgae kelp forests and seagrass meadows, which form biodiverse biogenic habitats (Schoch and Chenelot 2004; Alaska Department of Fish and Game 2015). Allochthonous nutrients are transported into the bay from oceanic sources and terrestrial runoff which spike robust seasonal primary productivity in spring and summer, and subsequent die-offs in the early boreal fall. The disparity of this nutrient input, however, runs along the bay from north to south and is affected by the inner and outer basin gyres separated by Homer Spit (Trasky et al. 1977). Thus, heterogeneity in primary productivity and ecosystem metabolism is separated in space (i.e., lengthwise along Kachemak Bay). The resultant biological metabolism along the bay fuels diurnal and seasonal O_2 and CO_2 variability, which play an integral part in coastal acidification (Baumann and Smith 2018; Feely et al. 2018; Pacella et al. 2018).

As a first-order chemical oceanographic characterization of the bay, this study details the first year of a multi-year study investigating high spatial and temporal variability of pH within enclosed bays along Kachemak Bay's inner and outer regions. The objectives were to catalogue the collected measurements into the Alaska Ocean Observing System (AOOS) database and elucidate the patterns and frequency of pH variability and potential drivers of these changes. We present data analysis of pH, O_2, temperature, and salinity in the time and frequency domains and detail an approach to determine accuracy and uncertainty when operating an deploying Sea-Bird Scientific's SeaFET™.

Methods

Study site and sensor deployment

Kachemak Bay is situated in the southeastern corner of Cook Inlet, Alaska. Two nearshore field sites—Jakolof Bay (59.466 N 151.534 W) and Bear Cove (59.726 N 151.056 W)—were selected for sensor package deployment (Fig. 1). These sites were chosen because they span the length of Kachemak

Fig 1. Geographical location of Kachemak Bay, Alaska, U.S.A., with sensor deployment sites in the outer and inner basin of Kachemak Bay. Jakolof Bay located toward the mouth (red circle) and Bear Cove (orange circle) at the head of the bay.

Bay, from the southern corner (outer basin) to the upper reaches of the bay (inner basin), bisecting the bay in a longshore axis. A sensor array outfitted with a Sea-Bird SeaFET™ pH sensor equipped with a copper cap placed over the electrodes (to prevent biofouling) and tributyltin plug was secured alongside a PME miniDOT optical oxygen logger and deployed at each site on 7–8 October 2017. Onset HOBO conductivity loggers were added to the sensor array on 19–20 December 2017. Jakolof Bay is located on the southern coast of Kachemak Bay and is notable for the diversity of invertebrate fauna (Lees et al. 1980). Bear Cove sits on the southeastern shore of Kachemak Bay, near the head of the bay. At Jakolof Bay, the sensor array was attached to a mooring frame, secured to a pier piling and placed roughly 1 m from the bottom in the shallow subtidal zone with up to 10 m of overlying water, depending on the tide. The Bear Cove sensor array was fastened to an anchor rope attached to a surface mooring that descended to a mid-water depth of 9 m in 23 m of water. This sensor array would shift closer to the bottom as the tide ebbed. Each site is located less than 100 m from the shoreline, and the distance between the two sites is 39.5 km. SeaFET™s were automated to sample every 3 h, with an average of 10 samples per frame (a single measurement averaged over 10 reads) and 30 frames per burst. Sampling measurements are reported here until 8 October 2018 with all timestamps reported in Coordinated Universal Time (UTC). Temperature measurements for each site were collected using the SeaFET™'s onboard thermistor.

Sensor calibration: Reference samples and measurements

SeaFET™ calibration and reference samples were collected from a single grab by diver's hand Niskin where sampling was proximate to each sensor array ~ 20 cm from the electrodes throughout the deployment period. The grab sample occurred within 30 s of the instrument sampling time period. Duplicate discrete bottle samples were filled from the single Niskin grab and measured as analytic replicates. In addition, sensor data was downloaded to check for anomalies, and a maintenance inspection was performed at every occurrence discrete samples were taken as part of a best practices protocol.

For Jakolof Bay, discrete seawater samples were collected on 20 December 2017, 00:00, 16 March 2018, 21:00, 10 June 2018, 00:00, and 14 August 2018, 18:00. The water sample collected on 20 Dec 2017 was used to calibrate sensor pH values, and the successive discrete samples were used as references to examine sensor uncertainty. Similarly, Bear Cove discrete water samples were collected on 19 Dec 2017, 21:00, 16 March 2017, 18:00, 7 June 2018, 21:00, and 13 August 2018, 18:00. The 16 March 2018 seawater sample was used to calibrate sensor pH values, and the following discrete samples were used to quantify pH uncertainty for this sensor. Samples were stored in 250 mL borosilicate bottles, fixed immediately with 200 μL saturated mercuric chloride, and were held in a refrigerator at $\sim 4^{\circ}$C until laboratory analysis. The pH_T (total scale) of each sample was measured at 25°C on a Shimadzu 1800 spectrophotometer (spectrophotometric method, SOP 6b, Dickson et al. 2007; using meta-cresol purple from Acros, batch # 30AXM-QN). A dye impurity correction factor (Douglas and Byrne 2017) was applied to the final calculation of pH_T. TA was measured via open-cell titration (A_T, SOP 3b, Dickson et al. 2007) using the Metrohm 848 Titrino plus. A YSI 3100 Conductivity instrument and handheld digital thermometer (Omega, HH81A) were used to measure salinity and temperature at the time of collection. pH_T in situ was calculated using CO2SYS (van Heuven et al. 2011) and the constants from Lueker et al. (2000), Uppström (1974), and Dickson et al. (1990) with the input parameters spectrophotometric pH_T (25°C) and TA (Table S1). Voltage measurements recorded by the SeaFET™ sensor were converted to pH_T as in Martz et al. (2010) using the single-point calibration method (Bresnahan et al. 2014; Miller et al. 2018) and Mathworks Matlab software (V. 2017a). This was done by using the measured pH_T from the discrete bottle samples and calculating the electrode specific single-point calibration coefficients, which were then used to derive each pH dataset. All pH_T reported values are from the internal SeaFET™ electrode given the accuracy, stability, and low inter-sensor variability associated with this electrode (Bresnahan et al. 2014; Gonski et al. 2018; Miller et al. 2018).

The HOBO-derived salinity data were calibrated using discrete bottle samples collected from each site and measured with a YSI 3100 conductivity meter. The subsequent data was postprocessed via HOBOware® Pro software using the laboratory measured discrete bottle samples that served as predeployment and postdeployment endmembers for each individual salinity dataset as per the manufacturer's recommendation.

Uncertainty and carbon chemistry estimates

The accuracy and uncertainty of the SeaFET™ sensor is dependent on intrinsic properties and user operation (*see* Miller et al. 2018 and references therein). In order to account for these potential sources of uncertainty, we calculated a propagated uncertainty and then applied this to the entire time series. Discrete bottle samples collected for calibration and reference points were scrutinized for overall accuracy based on uncertainty propagation. The individual sources of uncertainty are from spectrophotometric m-cresol dye, bottle replicates, titrator performance, and CO2SYS calculations. Uncertainty of spectrophotometric measurements with m-cresol were examined via triplicate analytical replicates using Certified Reference Material (CRM: Batch 172, A.G., Dickson, Scripps Institute of Oceanography). The mean value from the triplicate runs was integrated into a propagated uncertainty as m-cresol uncertainty. The standard deviation of measured pH_T from each discrete bottle sample served as bottle replicate uncertainty. Duplicate titrations were performed on each calibration and reference sample to address titrator uncertainty.

The TA standard deviation for each sample was then added to the difference between measured CRM and known CRM to calculate a titrator uncertainty as it affected pH_T. The final uncertainty term came from the calculation of in situ pH_T using TA and spectrophotometric pH_T at 25°C as input parameters to CO2SYS. This was calculated using the errors script (calculated using Matlab v2017a) linked with CO2SYS which outputs the error associated with deriving specific carbonate chemistry parameters based on the measured input parameters (Orr et al. 2018). The output uncertainty was given as H^+ concentration and recalculated as pH_T uncertainty. The following uncertainty propagation was summed in quadrature as:

$$Q = \sqrt{\sigma^2_{m-cresol} + \sigma^2_{Bottle\ replicates} + \sigma^2_{titrator} + \sigma^2_{CO2SYS\ constants}} \quad (1)$$

where Q is the propagated uncertainty, and σ is the standard deviation from all analytical calculations. This process was repeated each time discrete samples were taken. This uncertainty propagation of the measurement was then concatenated with the anomalies between discrete reference bottle pH_T and sensor pH_T. This was done by taking the mean of all uncertainty values and applying it as a total uncertainty across the entire time series (Table S2).

Estimates of TA values were determined for all time points where salinity data was available using the mean linear TA-salinity regression for the Gulf of Alaska (Evans et al. 2015; Siedlecki et al. 2017). TA estimates were then used alongside measured pH_T to constrain the carbonate system and estimate PCO_2 and aragonite saturation state (Ω_{arg}) using CO2SYS: constants Lueker et al. (2000), Uppström (1974), and Dickson et al. (1990). Uncertainty for these estimates was constructed by calculating PCO_2 and Ω_{arg} with CO2SYS using the minimum and maximum TA values at each site, this provided uncertainty end member values. The reported RMSE of 17.22 μmol kg^{-1} for the TA-salinity regression (Evans et al. 2015) was then subtracted from the maximum and minimum TA values to recalculate PCO_2 and Ω_{arg}. The difference between the original estimates and the recalculated PCO_2 and Ω_{arg} values was applied as a TA estimated uncertainty. The total uncertainty for the pH_T time series was then converted as a percent, and that proportion was then concatenated with the TA estimated uncertainty. This was done to account for the different units. A final uncertainty term was determined using the errors script (Matlab v2017a) associated with CO2SYS (Orr et al. 2018) for determining PCO_2 and Ω_{arg} from pH_T and TA.

pH time series and frequency analysis

To determine trends with seasonal changes and diurnal variability for the year-long deployment, pH_T was analyzed in the time domain to understand general patterns, while analysis in the frequency domain elucidated consistent frequencies in the magnitude of pH variability. Jakolof Bay time series data were corroborated against three discrete reference samples taken subsequent to the December calibration sample, whereas Bear Cove time series had two reference samples subsequent to the March 2018 calibration. pH_T time series was determined for both Jakolof Bay and Bear Cove sites across the entire deployment period, with monthly averages and a 30-day running average reported to depict monthly and seasonal trends in pH_T variability. The timing of pH_T variability is constrained by month in high-latitude regions due to sudden temperature changes and daylength, therefore, a power spectral density analysis for each month was performed on each pH_T time series using the pwelch function in Matlab (v2017a) with a sampling rate of 9.26×10^{-5} samples s^{-1}: equivalent to 8 samples d^{-1} (i.e., every 3 h). A Hanning window was applied to the pwelch function, and the mean pH_T value of each month was subtracted from the dataset in order to examine only the variance around the mean. A 3rd order Butterworth high-pass filter was designed and applied to the spectral analyses to remove any residual noise around a frequency of 0, which is an artifact of the transformation. The butter function in Matlab (v2017a) was set with a cut-off frequency of 1.00×10^{-5}. A power spectral density analysis breaks down the frequency components of the time series to reveal its underlying periodicity. The analysis displays what frequencies (i.e., the number of times per day a signal changes) have the greatest magnitude of variance. Months May through September coincide with subarctic primary production, and were the most variable with respect to pH_T (Welschmeyer et al. 1993; Strom et al. 2006). These months were analyzed at 12 h periods for nondirectional, cumulative, pH_T variability. The absolute difference in pH_T between 3 h increments over a 12 h period was calculated and summed. Time points from 00:00 to 12:00 and 12:00 to 00:00 were reported as half-day measurements of total pH_T variation for Jakolof Bay and Bear Cove sites.

Ancillary data analysis

Ancillary data such as temperature, salinity, and O_2 concentration were examined as drivers of pH_T variability and were analyzed in the time domain for both Jakolof Bay and Bear Cove datasets displaying associated pH_T values. The temperature from the internal SeaFET™ thermistor is reported in all analyses. Thermistor temperature was cross-validated with a handheld digital thermometer (Omega, HH81A) while the Jakolof Bay SeaFET™ was fully submerged in a sea-table at Kasitsna Bay laboratory. No offset was applied as this discrepancy in temperature (0.2–0.5°C) would affect pH_T to a degree lower than the precision of the instrument. Oxygen concentration and tidal amplitude were also correlated to the magnitude of pH_T variability for months May–September in the frequency domain via spectral analysis at both Jakolof Bay and Bear Cove sites. The same methods as above were used for these frequency transformations.

Residence time and water circulation can have an effect on pH_T variability and was included in ancillary data analyses.

Predicted tidal data was accessed from the National Oceanic and Atmospheric Administration (NOAA): tides and currents (https://tidesandcurrents.noaa.gov) for Kasitsna Bay and Bear Cove. Kasitsna Bay predictions were applied to the Jakolof Bay site as this was the closest prediction for this location. Tidal amplitude was calculated as the absolute difference from the mean lower low water and was examined as a predictor for pH_T variability. Tidal amplitude was collapsed because only the magnitude of deviation associated with pH variability was relevant to this study. Distinguishing specific patterns related to ebb and flood tides was outside the scope of this study as was the type of data needed for these analyses.

The net autotrophy and heterotrophy of the system were examined as correlatives of pH_T variability and were determined by comparing measured O_2 values against O_2 saturation. Oxygen saturation at atmospheric pressure was derived following the methods of Garcia and Gordon (1992) using measured temperature and salinity values. Apparent oxygen production was calculated as the difference between measured in situ concentration and saturation as a function of temperature and salinity. For periods where salinity was missing at Bear Cove, an estimated apparent oxygen production was determined from the average salinity taken over the entire time series where data points were present (19 December 2017–2018 May 2018). This method was deemed appropriate as salinity values from the Kachemak Bay National Estuarine Research Reserve reported salinity variability of ~ 2 units for all of 2017, and ~ 4 units (aside from a few anomalous spikes that appeared for only 15–30 min) for 2018 at the deep-water Homer Spit station (http://cdmo.baruch.sc.edu/dges/).

Statistical approach

Pearson's correlation coefficients were calculated between pH_T and factors temperature, tidal amplitude, and O_2 concentration for months May–September at Jakolof Bay and Bear Cove. Relationships were examined by month at every 3 h time point totaling 240 measurement points for a month with 30 d. The exact number of points varied based on day length per month and missing data points within a month.

The magnitude-squared coherence in the frequency domain was calculated between pH_T and factors tidal amplitude and O_2 concentration for months May–September at, both, Jakolof Bay and Bear Cove sites. The magnitude-squared coherence describes the power coherence between an input and output variable at a given frequency. Assuming a linear relationship of power variation exists between pH_T and tide amplitude and O_2 concentration, the magnitude-squared coherence assigns a correlation between pH_T and its driving factor at a specific frequency. Welch's approach (Welch 1967) of overlap segment averaging was applied with a 100-point Hanning window for determination of the magnitude-squared coherence. Prior to this analysis, cross-correlation between pH_T and each factor (i.e., tidal amplitude or O_2) was inspected to determine any potential lag time that could confound the correlation estimate. Because the resolution was every 3 h, the average of three time points (~ 45 min time-point^{-1}) around (± 1 time point), including the peak of the power spectral density, was used to determine the magnitude-squared coherence between O_2 concentration and tidal amplitude to pH_T.

Results

Apparatus performance

The sensor array at each site performed optimally with only a few mishaps in operation and data collection. The standard deviation between duplicate discrete bottle samples taken at Bear Cove on 19 December 2017 was > 0.05 pH units and, therefore, discarded as a nonrobust calibration or reference point (*see* Miller et al. 2018 for discussion on this threshold). This resulted in Bear Cove calibration with the 18 March 2018 sample, and one less discrete sample relative to Jakolof Bay. The conductivity logger attached to the sensor apparatus at Bear Cove malfunctioned in May with data logging failing after 18 May 2018. The sensor was not repaired or replaced, thus salinity data at Bear Cove was only collected from December 2017 to May 2018. During the June discrete sampling and maintenance inspection, sediment build was found in the copper cap of the Jakolof Bay SeaFET™ and the instrument was pulled for cleaning. This resulted in missing data points from 30 May 2018 to 10 June 2018. The sensor was redeployed on 11 June 2018, 00:00 after cleaning and proper operation verified. Prior to redeployment, the Jakolof Bay SeaFET™ was fully submerged in a sea table at Kasitsna Bay laboratory to test functionality for several days; thus, the discrete reference sample taken on 10 June 2018, 18:00 occurred in the wet lab rather than in the field. Given that the anomaly between this reference sample was greater than the in situ March reference, there is no indication that this sample was biased. A barnacle was found growing on the PME miniDOT at the Bear Cove site and was removed on June 2018. Any potential discrepancies in O_2 measurements during this time appear to be trivial as recognition of the exact time when barnacle attachment occurred could not be isolated relative to the background variability. Anomalous O_2 data showing erratic swings > 9 mg L^{-1} within a 3 h period at Bear Cove was observed at the beginning of September and was discarded for the rest of the time series. This was believed to be sensor malfunction as no other sensor showed irregularity at this time.

SeaFET™ accuracy and uncertainty

The discrete bottle samples used as reference points to verify SeaFET™ operation and accuracy were in fair agreement with SeaFET™ pH_T as anomalies were < 0.035 for Jakolof Bay and < 0.05 for Bear Cove (Table S2). The individual constituents of the propagated uncertainty values associated with the

measurement of the discrete bottle samples contributed minimally to overall pH_T uncertainty. Sources of uncertainty "bottle replicates" and "CO2SYS constant errors" accounted for the largest proportion of the total uncertainty value (Fig. S1, Table S2). The anomaly between the bottle samples and the SeaFET™ increased over time; however, the anomaly between the internal and external electrode remained consistent from June to August (~ 0.04 units) for both sensors and lacked any signs of biofouling build-up providing no clear explanation for the anomaly increase. The external electrode did not deviate from the internal electrode trend corroborating proper functionality of the sensors. The March reference sample for Jakolof Bay yielded the greatest propagated uncertainty, which was an order of magnitude higher than all other discrete samples. The total uncertainty applied to the entire Jakolof Bay times series was 0.0182, whereas Bear Cove total uncertainty was higher at 0.0210 (Table S2). This higher value for Bear Cove was due to the large anomaly between the SeaFET™ pH_T and the reference bottle sample taken during the August sampling period.

pH time and frequency variation

Each time series displayed distinct times of maximum and minimum pH_T values with extreme variability in September at Jakolof Bay and in June at Bear Cove. Jakolof Bay pH_T had little variation in fall 2017 through winter 2018 with a steady increase beginning in February and peaking around June: easily observable from the 30-day running average (Fig. 2a). Bear Cove pH_T had a range of 0.13 units from the beginning of the deployment until April, when a sharp rise in baseline pH_T and variability increased exponentially (Fig. 3a). The highest pH_T values here were observed at the very end of April and beginning of May, reaching a maximum of 8.37, which was 0.05 units greater than the maximum at Jakolof Bay in mid-June. A precipitous pH_T decline at Bear Cove began in late June and did not abate until October. The most significant decline in the 30-day running average was at a rate of 6% where pH_T dropped by 0.11 units in 19 d during the month of September (Fig. 3a). At Jakolof Bay, pH_T variability was greatest in September and during the first neap tidal cycle of that month (Figs. 2b, 4a). This was different at Bear Cove where

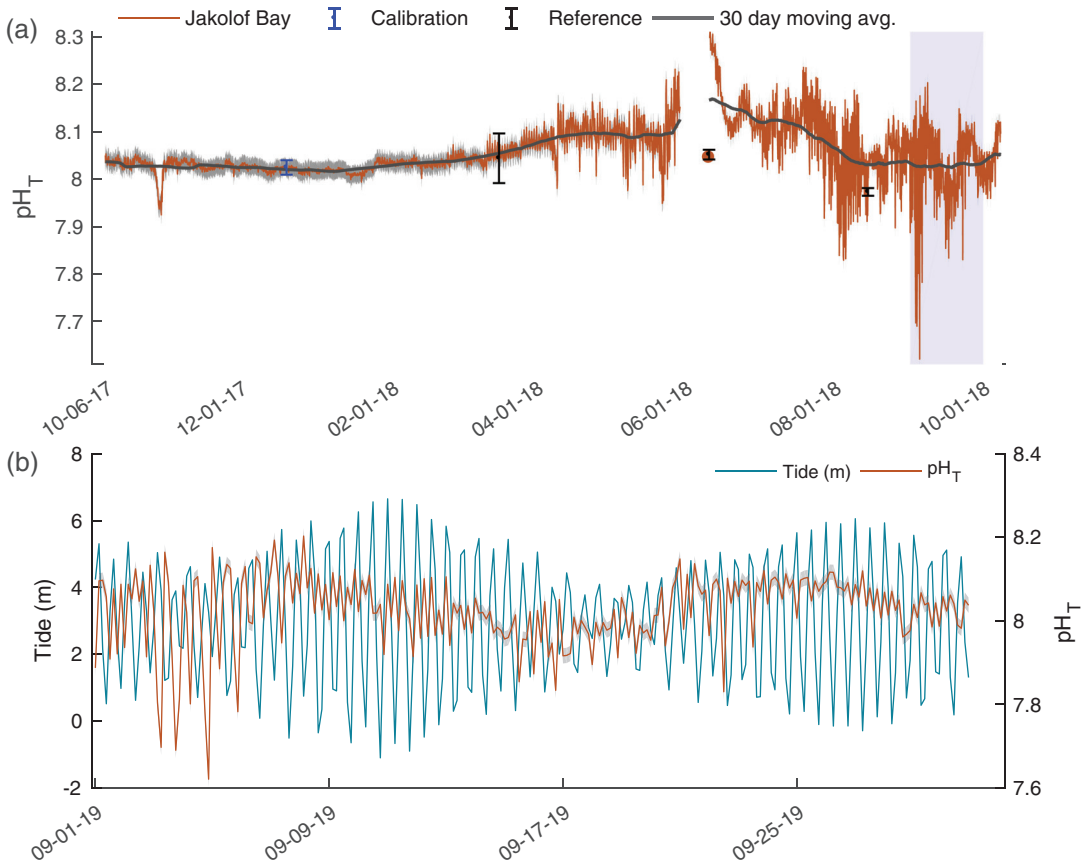

Fig 2. Times series of pH_T (**a**) from October 2017–October 2018 at Jakolof Bay. Black line is the 30-d running average with discrete bottle samples marked in blue (calibration time point) and black (reference samples) with standard deviations. Blue shaded region highlights the month of September, most variable month of pH_T at this location. Panel (**b**) is the shaded magnified region in the pH time series overlaid with predicted tidal height for the month of September. Gray shaded region around time series data is the propagated uncertainty (Table S2).

the transition from neap to spring tide coincided with greatest variability in pH_T at the end of May (Figs. 3b, 5a).

The variance around the monthly averages at both Jakolof Bay and Bear Cove differ in time and show distinct trends in seasonal variability and the frequency of diurnal variability. At Jakolof Bay the standard deviation of monthly pH_T means begin to increase in April and remain high through September (Fig. 4a). Bear Cove on the other hand only showed high variability for April, May, and June, where the variance was ≥ 2x the remaining months of the time series (Fig. 5a). Variability at both sites, however, increased with daylength. The magnitude of diurnal pH_T variability shown as power spectral density displayed notable peaks only during the months when pH_T was highly variable. Frequencies corresponding to 1, 2, and ~ 4 d^{-1} coincided with the strongest power spectral density values (Figs. 4b,c, 5b,c). September had the most robust power spectral density values at Jakolof Bay, and was the month with the greatest pH_T variation. Frequency peaks here were present at 0.6 (equivalent to a frequency signal once every 1.5 d) and ~ 3 in addition to 1, 2, and ~ 4 d^{-1} (Fig. 4b,c). Expectedly, the power spectral density peaks at Bear Cove where greatest during the month of May, which is congruent with high pH_T variance observed during this period (Fig. 5b,c). May and June shared similar frequency responses in pH_T variation with power spectral density peaks occurring approximately, 1, 2 and 0.5 d^{-1} (equivalent to once every 2.3 d). All other months did not display a power spectral density greater than 10 dB Hz^{-1} across all frequencies.

The summed absolute differences between each sequential 3 h pH_T measurement within a 12 h period displayed rapid shifts in pH_T at both sites. Over a 12 h period at Jakolof Bay, the total variation (i.e., summed positive and negative shifts) in pH_T was greatest for months August and September (Fig. 6a). On the fourth day of September, the total variation in pH_T over a 12 h period was > 1 full unit. June had the lowest variation in a 12 h period despite having a greater overall variance than the month of July (Fig. 6a). At Bear Cove, May and June had a similar magnitude in total pH_T variation over a 12 h period, however, the timing shifted throughout the month (Fig. 6b). In the first half of June the total variation in pH_T over a 12 h period reached a maximum of 0.5 pH_T units, whereas the second half of May had greater changes in pH_T reaching 0.54 units. The greatest magnitude of variation in May sustained for ~ 36 h from the 27th to 29th (Fig. 6b).

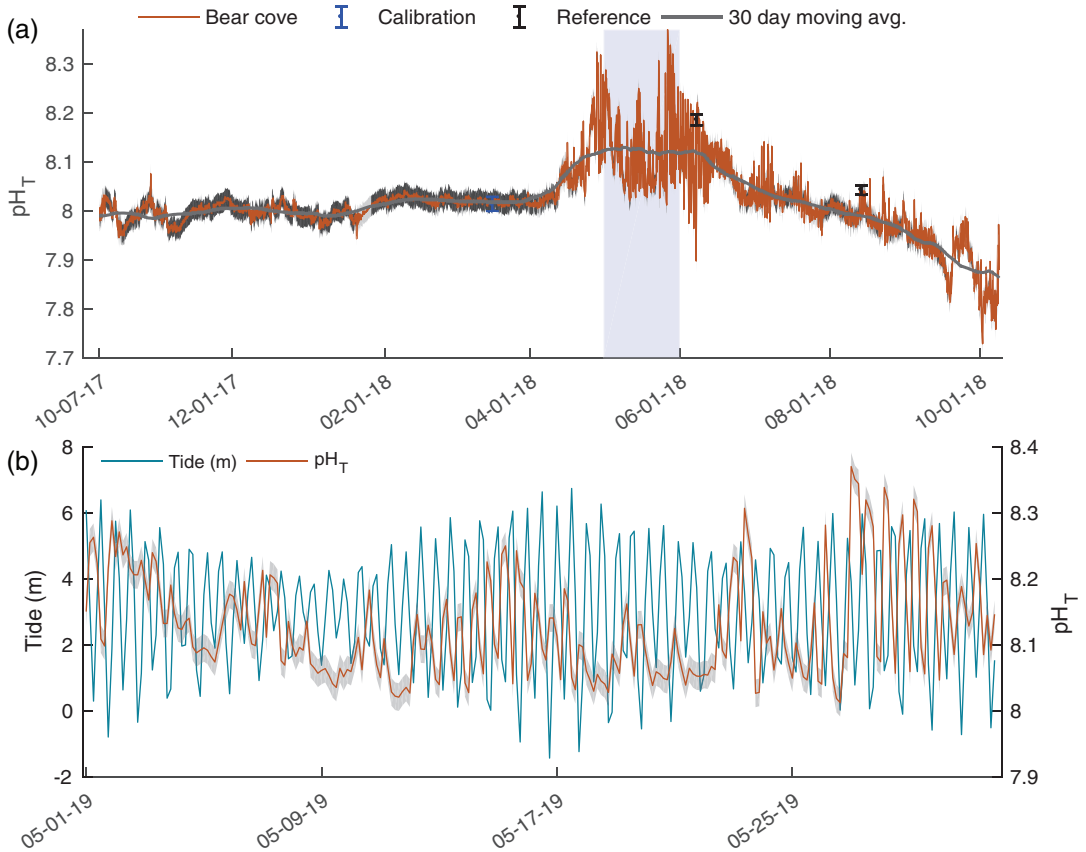

Fig 3. Times series of pH_T from October 2017 to October 2018 at Bear Cove (**a**). Black line is the 30-d running average with discrete bottle samples marked in blue (calibration time point) and black (reference samples) with standard deviations. Blue shaded region highlights the month of May, most variable month of pH_T at this location. Panel (**b**) is the shaded magnified region in the pH time series overlaid with predicted tidal height for the month of May. Gray shaded region around time series data is the propagated uncertainty (Table S2).

Trends in temperature, salinity, and oxygen

Temperature at Jakolof Bay followed a predictable seasonal trend with a dynamic range of 10°C reaching a low of 2.2°C in March and a high of 12.2°C in August (Fig. 7a). pH_T generally followed the temperature trend starting in January with lower values occurring in colder waters and higher pH_T in the warmer summer months. Deviations from this general trend occurred in early August and early September where pH_T appeared to deviate strongly from temperature resulting in low pH_T values relative to temperature (Fig. 7a). Temperature at Bear Cove was similar to Jakolof Bay ranging from 2°C to 12°C but with greater diurnal variability throughout the month of June (Fig. 8a). pH_T displayed very little variability from October 2017 to March 2018 despite a 10°C change in temperature during this period: the trend was similar to Jakolof Bay.

Salinity at Jakolof Bay fluctuated minimally from December 2017 through mid-July 2018 (Fig. 7b). Beginning on 22 July 2018, a repeated cyclical pattern of low salinity, ~25 occurred, every 24–27 h for about a week. On the 28th and 29th of July there were sustained lows averaging a salinity of 25. These somewhat stochastic events of low salinity appeared to have little or no effect on pH_T (Fig. 7b). The low salinity events coincided with an oncoming spring tide which likely transported a surface layer freshet that mixed with deeper water to drive the decline. With few exceptions, salinity at Bear Cove remained between 29 and 31 from August to October 2018 (Fig. 8b). Salinity increased ~2.5 units from December 2017 to April 2018 followed by stochastic variation ranging ~2 units until sensor failure in mid-May. pH_T appeared to be invariant relative to salinity at this time and remained at ~8.2 during the majority of the observed lower salinity values (Fig. 8b).

O_2 concentration slowly increased from the beginning of the deployment reaching a maximum of ~13.0 mg L^{-1} in June at Jakolof Bay (Fig. 7c). This gradual increase was interrupted by a drop in O_2 concentration beginning in mid-May where extreme stochasticity persisted for ~60 h until the second week of June (Fig. 7c). During June and July when oxygen concentrations where highest, diurnal variation was no greater than 1.5 mg L^{-1} and began a slow downward trend over these 2 months. pH_T appeared less sensitive to O_2 concentration during various points in June where pH_T differences of < 0.03 units corresponded to O_2 concentrations that varied ~3 mg L^{-1}. This decrease in pH_T

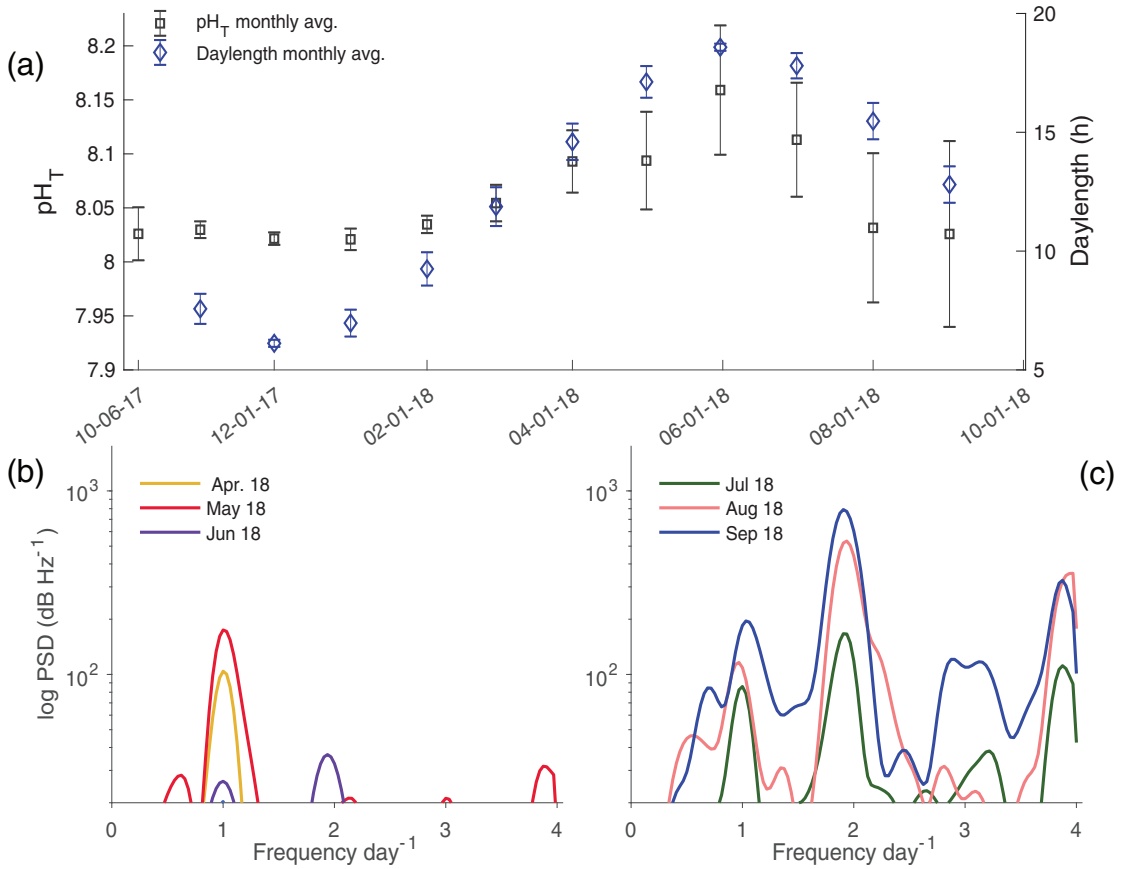

Fig 4. Monthly mean pH_T of Jakolof Bay time series from October 2017–September 2018 on the left y-axis with daylength on the right y-axis (**a**). Error bars are standard deviation. Power spectral density analysis of Jakolof Bay by month: April–June (**b**), and July–September (**c**). These months were the only ones with robust power spectral density magnitudes that exceed 20 dB Hz^{-1}. Months below this threshold are not shown.

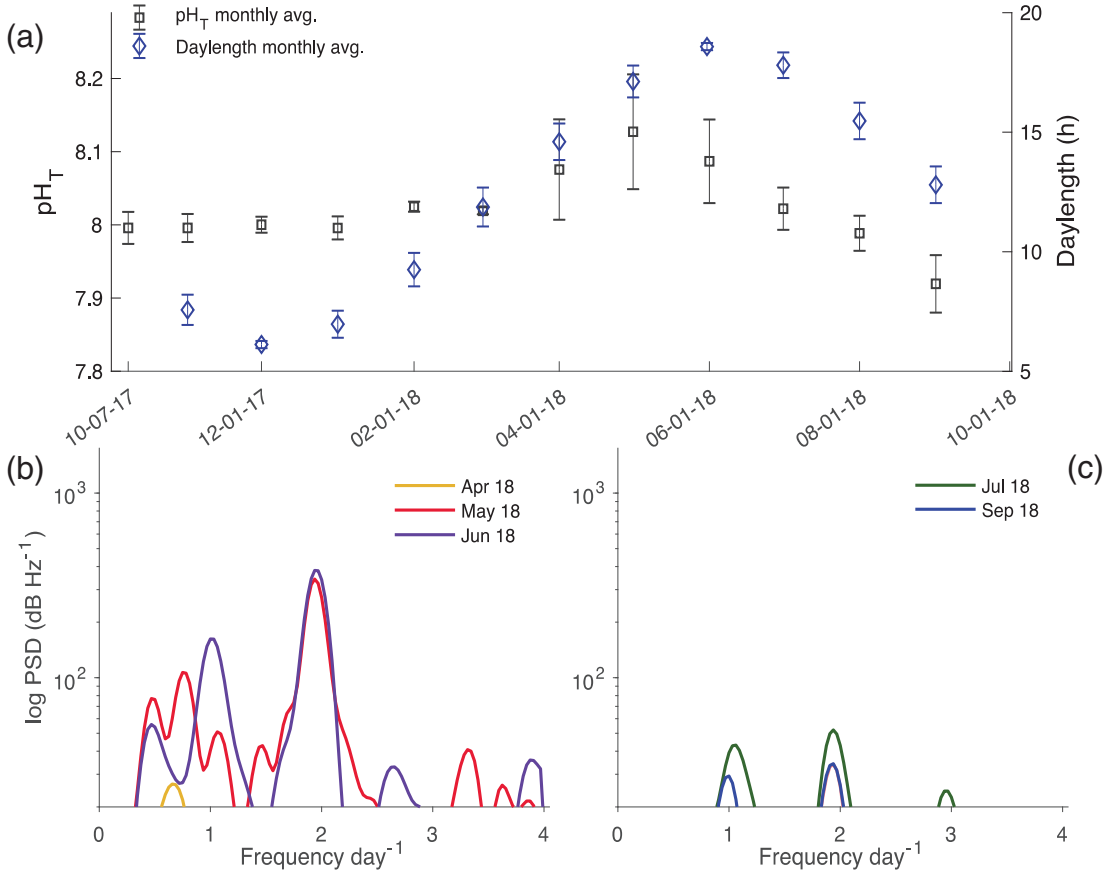

Fig 5. Monthly mean pH_T of Bear Cove time series from October 2017 to September 2018 on the left y-axis with daylength on the right y-axis (**a**). Error bars are standard deviation. Power spectral density analysis of Bear Cove by month: April–June (**b**), and July and September (**c**). These months were the only ones with robust power spectral density magnitudes that exceed 20 dB Hz^{-1}. Months below this threshold are not shown.

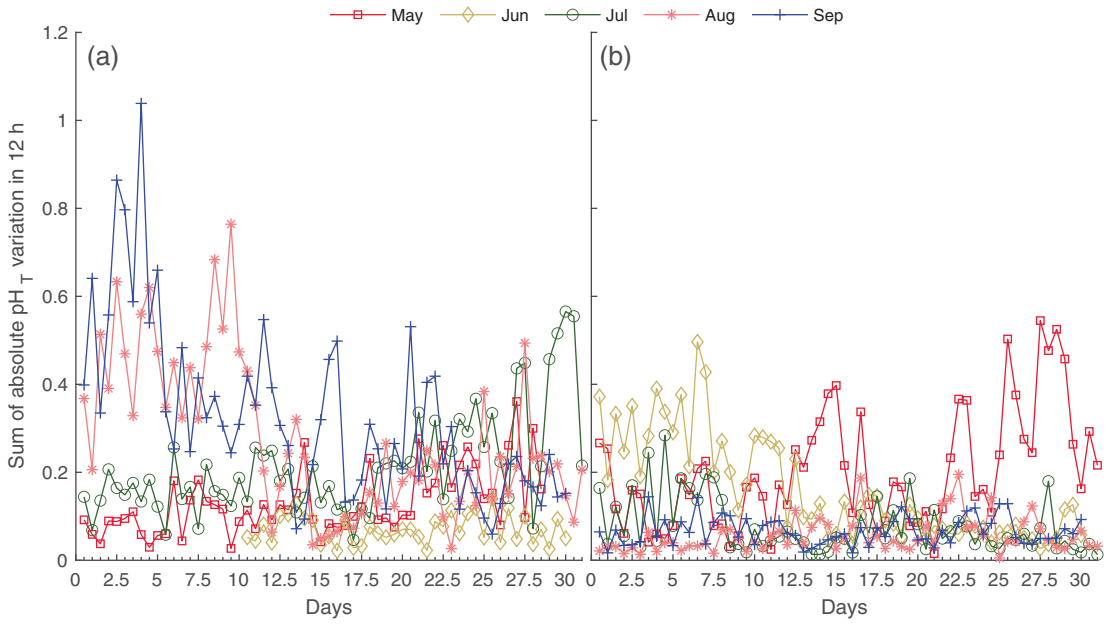

Fig 6. Nondirectional (i.e., $|pH_T - pH_{T+1}|$) sum of 3 h incremental measurements of pH_T variation every 12 h for months May–September at Jakolof Bay (**a**) and Bear Cove (**b**).

Fig 7. Time series of temperature (**a**), salinity (**b**), and oxygen (**c**) at Jakolof Bay. Colored markers are pH_T and gray markers are oxygen values where pH_T data is missing.

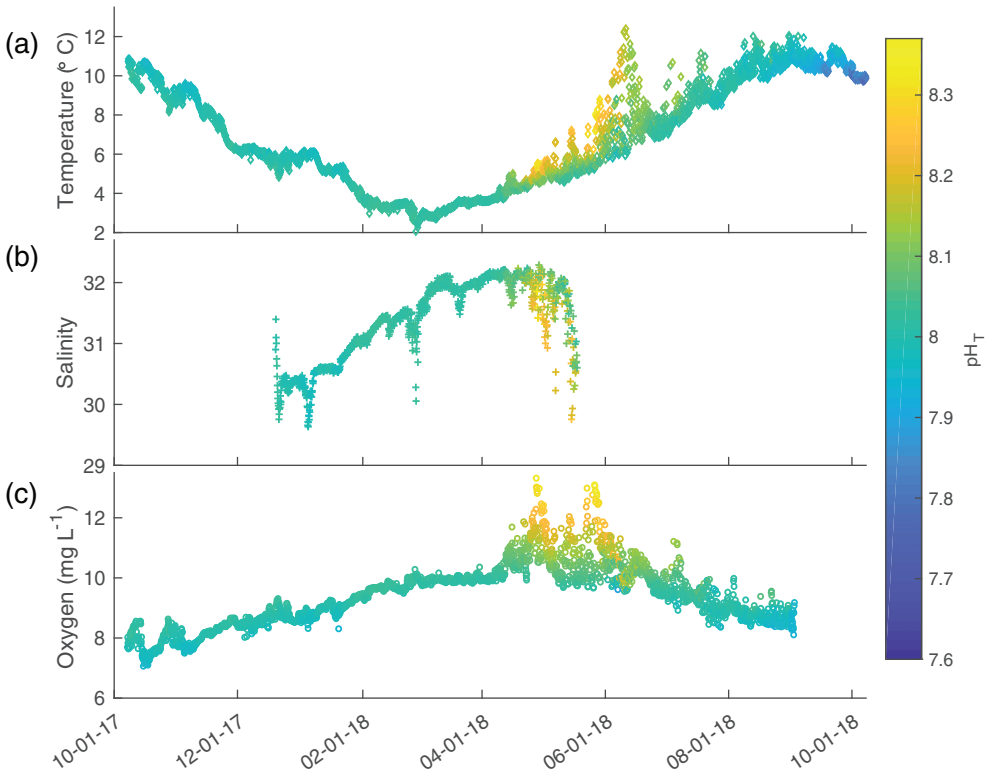

Fig 8. Time series of temperature (**a**), salinity (**b**), and oxygen (**c**) at Bear Cove. Colored markers are pH_T. Salinity measurements end on 18 May 2018 due to logger failure.

sensitivity appeared more prevalent during times of high O_2 concentration (Fig. 7c). O_2 concentration at Bear Cove was representative of primary production beginning in late spring, with cyclical variation ranging from 9.65 to 13.0 mg L^{-1} (Fig. 8c). During this period, pH_T appeared strongly coupled to the early spring variation in O_2 concentration (Fig. 8c).

The apparent oxygen production at Jakolof Bay was consistently greater than the solubility compensation point for a period of 2 months from mid-June to mid-August, which is indicative of a net autotrophic system (Fig. 9a). The low pH_T values in early September occurred below and above the O_2 solubility compensation. Calculation of apparent oxygen production at Bear Cove was only possible until the salinity logger malfunctioned in mid-May (Fig. 9b). O_2 concentration was greater than O_2 solubility for nearly all of May, and likely representative of a net autotrophic system during this time. This was converse to Jakolof Bay as O_2 began to rise earlier at Bear Cove than Jakolof Bay (Fig. 9). Estimated apparent oxygen production indicates that Bear Cove remained net autotrophic for the month of June until concentrations began to drop in July (Fig. 9c). Estimated apparent oxygen production was deemed viable since the discrepancy of O_2 saturation differed by ~ 0.3 mg L^{-1} over a salinity of 28–32 (range over all salinity data collected).

Correlations with pH variability

At Jakolof Bay pH_T correlation coefficients were, overall, low between pH_T and factors tidal amplitude, O_2 concentration, and temperature. The highest coefficients were observed in June for O_2 and temperature (Table S3). pH_T had the highest correlation with O_2, however, in September when pH_T was most variable, this correlation was at its lowest. While most correlation coefficients were significant, values were generally low and not robust.

For months May–August, correlation coefficients in Bear Cove between pH_T and O_2 concentration were >0.75: September correlations were removed due to anomalous O_2 data (Table S3). In September, pH_T had the greatest correlation with temperature at Bear Cove: $R = 0.83$. Both Jakolof Bay and Bear Cove sites displayed low correlation with tidal amplitude.

The magnitude-squared coherence between tidal amplitude and O_2 concentration with pH_T correlated well at Jakolof Bay from May to July (Fig. 10a). The power spectral density peaks during this time were consistent and occurred 1, 2 and ~ 4 times d^{-1}. The frequency of pH_T variation increased in August and September with new power spectral density peaks occurring every 0.5 and 3 times d^{-1}, approximately (Fig. 10a). At these frequencies in August, the magnitude-squared

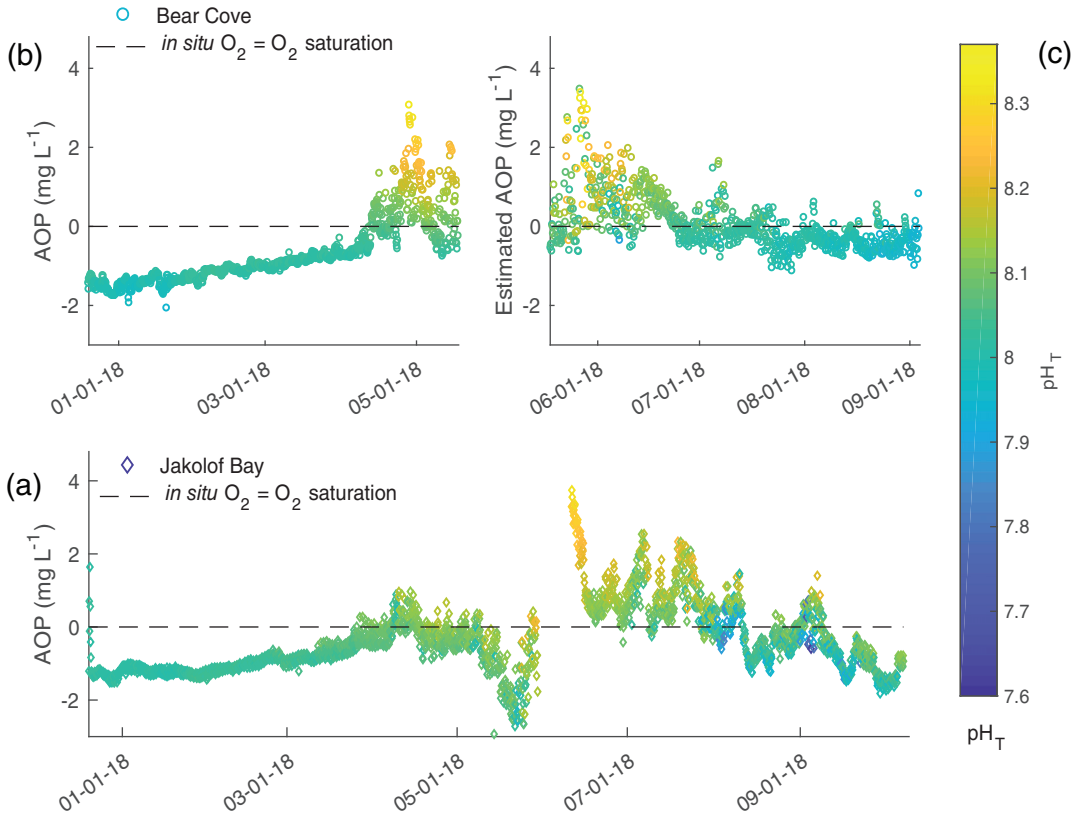

Fig 9. Times series of apparent oxygen production (i.e., measured $[O_2]_{in\ situ} - [O_2]_{saturation}$ ($\sim$ T, S)) for Jakolof Bay (**a**) and Bear Cove (**b**). Panel (**c**) is the estimated apparent oxygen production based on average salinity used to calculate $O_{2\ saturation}$ beginning 19 May 2018 after salinity logger failure. Colored markers are pH_T and dashed black line is when $O_{2\ saturation}$ is equal to $O_{2\ in\ situ}$.

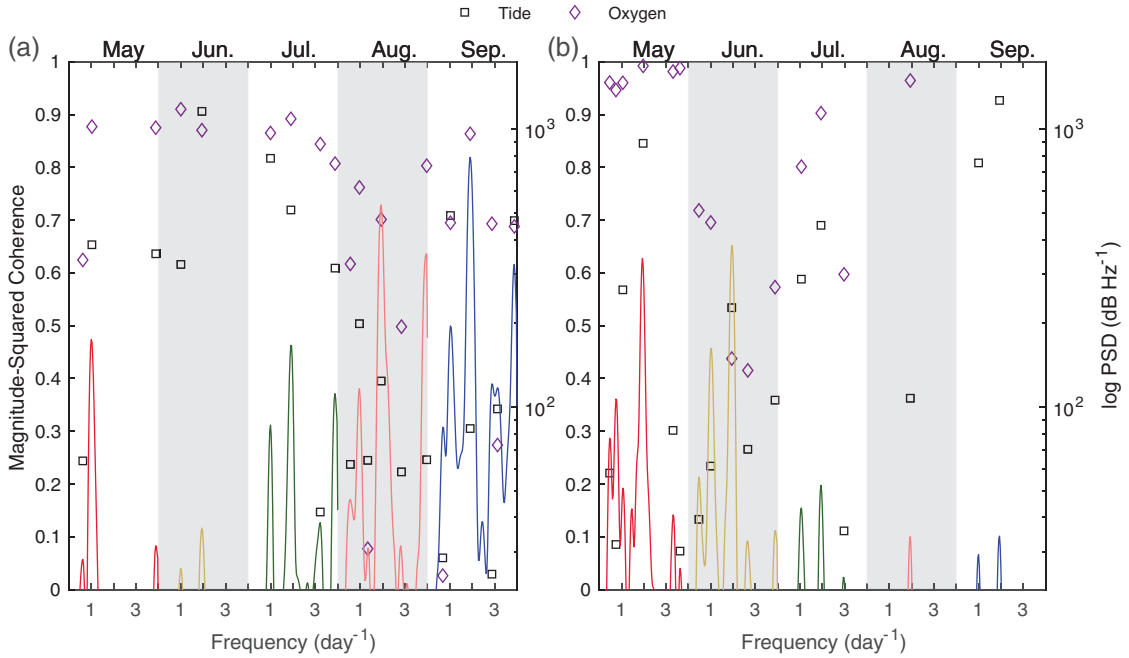

Fig 10. Magnitude-squared coherence at Jakolof Bay (**a**) and Bear Cove (**b**) on the left y-axis between pH_T and oxygen (purple diamonds) and tidal amplitude (black squares) as it corresponds to each peak in the power spectral density for pH_T (right y-axis). Shaded regions distinguish separation of months.

coherence between O_2 and pH_T was ≥ 0.5 compared to tidal amplitude and pH_T, which was less than 0.3. The power spectral density peaks at Jakolof Bay were most abundant in September. The magnitude-squared coherence between tidal amplitude and O_2 with pH_T were similar across most peaks in September, with the exception of frequencies 1.91 and 2.88 d^{-1} where the O_2 magnitude-squared coherence was at least > 2.5× the magnitude-squared coherence between tidal amplitude and pH_T.

The magnitude-squared coherence between pH_T and tidal amplitude at Bear Cove was >0.5 at frequencies approximately 1 and 2 d^{-1} with exceptions occurring in June at ~ 1 d^{-1}, and in August at 2 d^{-1} (Fig. 10b). May and June had the greatest number of power spectral density peaks outside the frequencies of 1 and 2 d^{-1}. These other frequencies (i.e., frequencies other than 1 and 2 d^{-1}) displayed a high magnitude-squared coherence with O_2 concentration and were abundant in May and June (Fig. 10b). Overall, consistent frequency patterns in pH_T for July–September at Bear Cove were minimal.

Trends of carbonate chemistry estimates

Estimates of carbonate chemistry parameters PCO_2 and Ω_{arg} follow expected trends with pH_T values and reflect the extreme variability of carbonate chemistry in the summer months (Fig. S2). At Jakolof Bay a maximum Ω_{arg} of 2.98 was calculated in June, while a minimum Ω_{arg} of 0.73 calculated in September (Fig. S2b). PCO_2 estimates ranged between 185 μatm in June to 1095 μatm in September. At Bear Cove, PCO_2 and Ω_{arg} were likely more extreme than what was recorded becasue maximum pH_T was at the end of May and estimations only extended to 18 May 2018 due to missing salinity data (Fig. S2a). Despite a greater amount of uncertainty with these estimates, which is a PCO_2 of ± 16 and 23 μatm for Jakolof Bay and Bear Cove, respectively, and an Ω_{arg} of ~ 0.13, there is a fair amount of confidence that the true values fall within the uncertainty bounds which display rapid changes in both parameters (Fig. S2).

Discussion

Seasonal trends and extremes with high signal-to-noise

Presented here is the first account of year-long, high temporal-resolution, pH time series collected in an Alaskan estuary beginning in October of 2017. Jakolof Bay which is situated in the outer basin of Kachemak Bay experienced greater pH and O_2 variability—which occurred for longer durations—than Bear Cove. Maximum pH_T values were > 8.3 with a minimum of 7.6 units at Jakolof Bay. For nearshore systems, Kachemak Bay pH dynamics rank close to the most variable sites on the U.S. west coast with respect to rates of hourly pH change: observed to be as high as ~ 0.2 h^{-1} in Jakolof Bay (Hofmann et al. 2011; Chan et al. 2017; Baumann and Smith 2018). High rates of pH variability were present only seasonally and concurrent with high rates of O_2 production indicative of a system whose carbonate chemistry is dominated by biological processes. Recent studies have shown that biological metabolism is a strong seasonal driver of pH dynamics and is a factor that can lead to short-term extremes of acidification and seawater corrosivity (Feely et al. 2018;

Pacella et al. 2018; Lowe et al. 2019). We find that Kachemak Bay is one such location where seasonal pH patterns are predominately driven by biological metabolic cycles. Therefore, this study recommends methods aimed at elucidating accuracy and nuance to extreme short-term fluctuations in pH as mediated by biology, by accounting for all constituents of uncertainty and identification of the frequency at which variability is observed.

Instilling a robust uncertainty protocol is essential to determine the accuracy of rapid changes in pH. For example, the total uncertainty calculated for Jakolof Bay was 0.0184 (Table S2) which is < 10% of the greatest rate in hourly change observed at this site. The low uncertainty provides the ability to report small rapid changes in pH whereas high uncertainty would not be able to accurately capture such fluctuations. The importance of a signal-to-noise ratio has been highlighted elsewhere as a method for detecting trends (Kapsenberg and Hofmann 2016; Carter et al. 2019), and is reiterated here if small rapid changes in pH are to be identified and reported. With respect to detecting future trends in this system, the importance of reducing sources of uncertainty will be imperative for detecting emergent patterns of anthropogenic acidification and incorporating this region into the GOA-ON database. Currently, the degree of uncertainty around the measurement of acidification parameters distinguishes a difference between datasets reporting "weather" or "climate" to be 0.02 and 0.003 pH units, respectively (Newton et al. 2015). Both Jakolof Bay and Bear Cove have total uncertainty values that are ± 0.002 pH units around the 0.02 threshold categorizing both locations with weather accuracy (Table S2). It is important to note that the relative variability across months and a proportion of pH variability within a 12 h period have robust signal-to-noise ratios validating confidence in reported measurements despite an uncertainty slightly > 0.02 for Bear Cove. The uncertainty estimate for Bear Cove, however, was lacking a reference sample which could have decreased or increased the estimate. The most probable reason for the discrepancy of the December Bear Cove bottle sample was likely due to improper sample preservation as the TA measurements also displayed a large anomaly (Table S1).

Modification of pH by photosynthesis and respiration

The unique oceanography of Kachemak Bay due in part to its bifurcation make this region an important location to characterize in the context of global ocean change. Both Jakolof Bay and Bear Cove have strong spikes in pH that occur with increased oxygen production and follow cyclical patterns. The seasonal increases in pH were temporally dissimilar between sites as pH maxima in Jakolof Bay and Bear Cove were in June and May, respectively. The greatest 12 h period of total variability was also disparate between sites as Jakolof Bay experienced greatest variability in September when this system transitioned from net autotrophic to net heterotrophic. Conversely, Bear Cove experienced maximum variability in May during the system's transition from net heterotrophic to net autotrophic. The balance between community respiration and photosynthesis appears to be the driver of seasonal pH extremes and variability at both sites and is further dependent on the biota at each location. Primary production in Jakolof Bay is driven by a mix of microalgae and macroalgae where dense kelp beds of *Saccharina latissima* are extensive with annual bloom and die-off cycles (Dames and Moore 1977). Bear Cove lacks such macroalgae assemblages and productivity is driven more by phytoplankton sources. This aspect of divergent patterns of primary producers may correlate with two observed seasonal patterns in pH variability, with the caveat that kelp dominated systems increase pH dynamics in arctic systems (Krause-Jensen et al. 2015). First, Bear Cove pH and O_2 began to increase earlier in the season than Jakolof Bay. Macroalgae recruitment and growth is slower than phytoplankton as longer residence times in the inner basin likely promote greater phytoplankton abundance over macroalgae present in the outer basin (Field and Walker 2003; Wallace and Gobler 2015). Second, Jakolof Bay experiences a stochastic pH pattern in September relative to Bear Cove. Total variability of pH_T over a 12 h period reached a magnitude > 1 unit during September in Jakolof Bay—this was nearly double that observed in Bear Cove's most variable pH month, which was May. This pattern of pH decline and minima in the fall at Jakolof Bay coincides with the die-off of large, fleshy, macroalgae beginning in July. While O_2 concentration is also variable during September, lower concentrations would be expected due to increased heterotrophy during macroalgae demise in order to correlate with the low pH values; however, extremely low pH_T values were observed with moderate O_2 concentrations in September indicating a temporal mismatch between these two parameters. To reiterate, the extreme fluctuations observed in September are likely the transition of the system to net heterotrophic after an approximate 60 d period as being net autotrophic. It is suggested here that the increase in heterotrophy in September is likely correlated to macroalgae demise; and the moderate O_2 levels during this time may be a shift back to increases in phytoplankton abundance and photosynthesis as macroalgae declines and surface irradiance coverage and penetration increases with canopy loss (Miller et al. 2011).

The more extreme fluctuations in pH at Jakolof Bay are not only due to the type of primary producer, but greater biomass overall. The outer basin of Kachemak Bay is more coupled to the greater Gulf of Alaska. These conditions facilitate nutrient delivery and dispersal of fauna (Field and Walker 2003). From May to September, correlations between pH and O_2 concentration were weaker at Jakolof Bay compared to Bear Cove (Table S3). This may also be explained by the geography of this region as the inner basin has longer residence times and lower biomass resulting in greater O_2 mediated changes in pH, rather than the continual fluctuation of high respiration and photosynthetic cycles occurring in the background of more robust mixing. Physical drivers of pH, however, did not appear

to affect either location disproportionately relative to the biological signal. This can be seen as pH rises steadily with temperature until O_2 production and respiration create consistent variability lasting until fall. Overall pH at either site did not appear to respond to salinity fluctuations, and salinity dynamics were low even at Bear Cove which historically receives more freshwater input than Jakolof Bay (Trasky et al. 1977; Field and Walker 2003). Given that Jakolof Bay predominately follows physical oceanic trends similar to the Gulf of Alaska, which can experience seasonal upwelling, there was no evidence of upwelling in the temperature and salinity signature. Both sites are shallow tidal estuaries with large inlets making any upwelling signal extremely diffuse if existent at all, and this was verified by aligning pH with the upwelling index at 60°N and 149°W (https://www.pfeg.noaa.gov) (e.g., Fig. S3).

Understanding the frequency of pH variability

Drivers of pH variability whether physical or biological (e.g., temperature and O_2) are not mutually exclusive and act to define the frequency at which pH variability occurs. Seasonal shifts and diurnal pH variability in response to temperature increases, biological metabolism, and riverine discharge have been extensively addressed when providing context to experimental design and the frequency of pH variability (Cornwall et al. 2013; Joesoef et al. 2017; Van Dam and Wang 2019). The frequency of carbonate chemistry variation, however, can occur on much shorter time scales as described here, and can potentially overlap with biological sensitivities to acidification which have been shown to occur on the time scale of hours (Waldbusser and Salisbury 2014; Waldbusser et al. 2015; Kapsenberg et al. 2018). Observations here show that this hourly scale in the frequency of variability during the months of May–September displayed nearly consistent peaks at 1, 2, $\sim 4\ d^{-1}$, likely associated with the semi-diurnal tidal signal. This trend is unequivocal when looking specifically at the power spectral density analysis for tidal amplitude where three peaks are present and believed to correspond to the mixed semi-diurnal tides (Fig. S4). The expected fourth peak for the tide power spectral density is absent as it would occur minutes past the 24 h period. The importance of this phenomenon shows the degree to which such large mixed semi-diurnal tidal exchanges can spike pH variability in either the positive or negative direction depending on the flood water and the biologically modified source water within the estuary. It would be expected that given the tidal prism and biological metabolism occurring within the estuary, that these two drivers potential nullify the other's effect. The interplay between biological metabolism and tidal amplitude can be seen in the most variable months at Jakolof Bay and Bear Cove which had multiple peaks in daily pH variability, likely driven by nontidal signatures.

Correlations with pH variability in frequency domain

To help determine the frequency and drivers of pH variability we applied a novel approach to correlate the power spectral density of pH with O_2 and tidal amplitude. Recent studies have highlighted the importance of correlating physical and biological conditions associated with nearshore pH variability, and emphasize the need to incorporate these data when examining and reporting pH observations (Kapsenberg and Hofmann 2016). Thus far, correlations between carbonate chemistry in the time domain with ancillary oceanographic data have not provided the temporal resolution needed to identify the frequency of semdiurnal and diurnal variability in the Gulf of Alaska region (Evans et al. 2015; Reisdorph and Mathis 2015; Siedlecki et al. 2017). Analyses in this study show clear correlations between peak pH variability with tidal amplitude and O_2 over a diurnal scale which identifies specific hourly frequencies of O_2 or tidal driven pH variability. While there is likely collinearity between pH and O_2 with tidal amplitude at specific frequencies (e.g., 1 and $2\ d^{-1}$), there are clear instances where the magnitude-squared coherence between pH and oxygen is > 5× that of tidal amplitude, such as in September at a frequency of $\sim 3\ d^{-1}$ in Jakolof Bay. This signal suggests that biological metabolism is the driving source of pH variability at $3\ d^{-1}$, which could correspond to excessive photosynthesis and respiration cycles following the photoperiod of that month. Understanding these peak frequencies of variability is imperative when trying to identify acute events of unfavorable water chemistry as short windows of stressful conditions have been shown to reduce growth and development of sensitive larval bivalves (Waldbusser et al. 2015). For example, bivalve out-planting projects may benefit from knowing which months are most favorable with respect to pH, and relying on a previous year's times series may vary dramatically from year-to-year, but the frequency of pH variability would likely remain more consistent, although with differing levels of magnitude. Previous analyses have highlighted the importance of identifying frequency changes in carbonate chemistry, and the data here aim to address some of these gaps in knowledge (Waldbusser and Salisbury 2014). In addition, the frequency of pH variability driven by biological metabolism could act in a synergistic or additive way to large-scale anomalous events such as riverine discharge (McCutcheon et al. 2019). Without properly incorporating short-term frequency variability, conclusions drawn from large-scale anomalies of pH and carbonate chemistry may be inaccurate with respect to the resolution of rapid changes.

Correlation between tidal amplitude and pH were low overall when examined in the time domain (Table S3). Given the amplitude of tides in Kachemak Bay, it was hypothesized that pH would correlate well with tidal amplitude, however, this was not the case. Close examination revealed that correlations on the monthly scale where likely too coarse to identify robust correlations. During the months of high pH variability (May–September), any tidal signal was likely out-weighed by the response of pH to O_2. In other words, the disparity between tidal and oxygen coherence in relation to pH is indicative of O_2 production dominating without tidal dilution or flushing.

Additionally, it appeared that pH variability was lower during spring tides than neap tides for months May, June and September in Jakolof Bay. However, statistical evaluation was unclear as there was no consistency in a higher coefficient of variation value of pH when splitting months by spring and neap tidal cycles. It would be remiss to say that there is no relationship between pH variability and tidal amplitude as one was clearly identified in the frequency domain, but rather that O_2 was a dominant driver of pH on the monthly scale. Wind speed is another potential factor that can affect the frequency of pH variability by changing the rate of the sea-air CO_2 flux (Wanninkhof 2014; Xue et al. 2018; Pilcher et al. 2019). Correlations were, therefore, examined between pH variability and wind speed measured by the Kasitsna Bay National Estuarine Research Reserve station on Homer Spit (http://cdmo.baruch.sc.edu/dges/) with results showing no observable pattern or association. This likely indicates that these nearshore water masses are well mixed as a result of the strong tidal prisms in Kachemak Bay; or in the case of Bear Cove, wind speed measurements on Homer Spit were not representative of this enclosed, inner basin, bay.

Conclusion

The frequency patterns of pH variability presented here are likely to increase in magnitude under future acidification scenarios where extreme values will become greater and the rates of short-term change will increase (Gruber et al. 2012; Hauri et al. 2013; Waldbusser and Salisbury 2014). Further, the importance of correlating the frequency of pH variability with the mechanisms inducing pH change is critical when identifying potential sensitivities to acidification, resilience, and adaptive capacity. In the context of ecosystem function in a changing ocean, the frequency of extreme pH conditions observed here may act as an environmental history that enhances adaptive capacity, referred to as OA refugia, or exacerbate acidification conditions pushing organisms already found at the extremes of their physiological thresholds into deleterious conditions (Waldbusser and Salisbury 2014; Kapsenberg and Cyronak 2019). In order to enhance the spatiotemporal assessment presented here, efforts are currently being pursued to expand the current sensor network throughout the great Kachemak Bay region, which will enhance the understanding of ocean change in important subarctic marine ecosystems.

References

Alaska Department of Fish and Game. 1998. Kachemak Bay National Estuarine Research Reserve (KBNERR). Management plan, operations and development: Environmental impact statement [accessed 2019 September 2]. Available from https://catalog.hathitrust.org/Record/100982187.

Alaska Department of Fish and Game. 2015. Wildlife action plan appendix 5: Marine and coastline habitats.

Alaska Department of Fish and Game. Habitat and Restoration Division. 2001. Kachemak Bay ecological characterization. The Center, [Print].

Bandstra, L., B. Hales, and T. Takahashi. 2006. High-frequency measurements of total CO_2: Method development and first oceanographic observations. Mar. Chem. **100**: 24–38. doi:10.1016/j.marchem.2005.10.009

Baumann, H., and E. M. Smith. 2018. Quantifying metabolically driven pH and oxygen fluctuations in US Nearshore habitats at diel to interannual time scales. Estuaries Coasts **41**: 1102–1117. doi:10.1007/s12237-017-0321-3

Beckwith, S. T., R. H. Byrne, and P. Hallock. 2019. Riverine calcium end-members improve coastal saturation state calculations and reveal regionally variable calcification potential. Front. Mar. Sci. **6**. doi:10.3389/fmars.2019.00169

Bresnahan, P. J., T. R. Martz, Y. Takeshita, K. S. Johnson, and M. LaShomb. 2014. Best practices for autonomous measurement of seawater pH with the Honeywell Durafet. Methods Oceanogr. **9**: 44–60. doi:10.1016/j.mio.2014.08.003

Carter, B. R., N. L. Williams, W. Evans, A. J. Fassbender, L. Barbero, C. Hauri, R. A. Feely, and A. J. Sutton. 2019. Time of detection as a metric for prioritizing between climate observation quality, frequency, and duration. Geophys. Res. Lett. **46**: 3853–3861. doi:10.1029/2018GL080773

Chan, F., and others. 2017. Persistent spatial structuring of coastal ocean acidification in the California current system. Sci. Rep. **7**: 2526. doi:10.1038/s41598-017-02777-y

Cornwall, C. E., C. D. Hepburn, C. M. McGraw, K. I. Currie, C. A. Pilditch, K. A. Hunter, P. W. Boyd, and C. L. Hurd. 2013. Diurnal fluctuations in seawater pH influence the response of a calcifying macroalga to ocean acidification. Proc. R. Soc. B: Biol. Sci. **280**: 20132201. doi:10.1098/rspb.2013.2201

Dames and Moore Group (URS corp.). 1977. Final report: Reconnaissance of the intertidal and shallow subtidal biota lower cook inlet. National Oceanic and Atmospheric Administration.

Dickson, A. G., D. J. Wesolowski, D. A. Palmer, and R. E. Mesmer. 1990. Dissociation constant of bisulfate ion in aqueous sodium chloride solutions to 25°C. J. Phys. Chem. **94**: 7978–7985. doi:10.1021/j100383a042

Dickson, A. G., C. L. Sabine, and J. R. Christian. 2007. Guide to best practices for ocean CO_2 measurements, v. **3**. North Pacific Marine Science Organization. [PICES Special Publication].

Douglas, N. K., and R. H. Byrne. 2017. Achieving accurate spectrophotometric pH measurements using unpurified *meta*-cresol purple. Mar. Chem. **190**: 66–72. doi:10.1016/j.marchem.2017.02.004

Dugan, D., C. Janzen, M. McCammon, W. Evans, and A. Bidlack. 2017. The evolution of ocean acidification observing efforts in Alaska and the development of an Alaska

Ocean acidification network, p. 1–6.*In* OCEANS 2017—Anchorage. Institute of Electrical and Electronics Engineers.

Ekstrom, J. A., and others. 2015. Vulnerability and adaptation of US shellfisheries to ocean acidification. Nat. Clim. Change **5**: 207–214. doi:10.1038/NCLIMATE2508

Evans, W., J. T. Mathis, and J. N. Cross. 2014. Calcium carbonate corrosivity in an Alaskan inland sea. Biogeosciences **11**: 365–379. doi:10.5194/bg-11-365-2014

Evans, W., J. T. Mathis, J. Ramsay, and J. Hetrick. 2015. On the frontline: Tracking ocean acidification in an Alaskan shellfish hatchery. PLoS One **10**: e0130384. doi:10.1371/journal.pone.0130384

Fabry, V. J., J. B. McClintock, J. T. Mathis, and J. M. Grebmeier. 2009. Ocean acidification at high latitudes: The bellwether. Oceanography **22**: 160–171. doi:10.5670/oceanog.2009.105

Feely, R. A., R. R. Okazaki, W.-J. Cai, N. Bednaršek, S. R. Alin, R. H. Byrne, and A. Fassbender. 2018. The combined effects of acidification and hypoxia on pH and aragonite saturation in the coastal waters of the California current ecosystem and the northern Gulf of Mexico. Cont. Shelf Res. **152**: 50–60. doi:10.1016/j.csr.2017.11.002

Field, C., and C. Walker. 2003. A site profile of the Kachemak bay research reserve: A unit of the National Estuarine Research Reserve System. Kachemak Bay Research Reserve.

Garcia, H. E., and L. I. Gordon. 1992. Oxygen solubility in seawater: Better fitting equations. Limnol. Oceanogr. **37**: 1307–1312. doi:10.4319/lo.1992.37.6.1307

Gonski, S. F., W.-J. Cai, W. J. Ullman, A. Joesoef, C. R. Main, D. T. Pettay, and T. R. Martz. 2018. Assessment of the suitability of Durafet-based sensors for pH measurement in dynamic estuarine environments. Estuarine Coast. Shelf Sci. **200**: 152–168. doi:10.1016/j.ecss.2017.10.020

Gruber, N., C. Hauri, Z. Lachkar, D. Loher, T. L. Froelicher, and G.-K. Plattner. 2012. Rapid progression of ocean acidification in the California current system. Science **337**: 220–223. doi:10.1126/science.1216773

Hales, B., D. Chipman, and T. Takahashi. 2004. High-frequency measurement of partial pressure and total concentration of carbon dioxide in seawater using microporous hydrophobic membrane contactors. Limnol. Oceanogr.: Methods **2**: 356–364. doi:10.4319/lom.2004.2.356

Hauri, C., N. Gruber, A. M. P. McDonnell, and M. Vogt. 2013. The intensity, duration, and severity of low aragonite saturation state events on the California continental shelf. Geophys. Res. Lett. **40**: 3424–3428. doi:10.1002/grl.50618

Hofmann, G. E., et al. 2011. High-frequency dynamics of ocean pH: A multi-ecosystem comparison. PLoS One **6**: e28983. doi:10.1371/journal.pone.0028983

Joesoef, A., D. L. Kirchman, C. K. Sommerfield, and W. J. Cai. 2017. Seasonal variability of the inorganic carbon system in a large coastal plain estuary. Biogeosciences **14**: 4949–4963. doi:10.5194/bg-14-4949-2017

Kapsenberg, L., and T. Cyronak. 2019. Ocean acidification refugia in variable environments. Glob. Chang. Biol. **25**: 3201–3214. doi:10.1111/gcb.14730

Kapsenberg, L., and G. E. Hofmann. 2016. Ocean pH time-series and drivers of variability along the northern Channel Islands, California, USA. Limnol. Oceanogr. **61**: 953–968. doi:10.1002/lno.10264

Kapsenberg, L., A. Miglioli, M. C. Bitter, E. Tambutté, R. Dumollard, and J. P. Gattuso. 2018. Ocean pH fluctuations affect mussel larvae at key developmental transitions. Proc. R. Soc. B: Biological Sciences **285**: 20182381. doi:10.1098/rspb.2018.2381

Kelley, A. L., and J. J. Lunden. 2017. Meta-analysis identifies metabolic sensitivities to ocean acidification. Environ. Sci. **4**: 709–729. doi:10.3934/environsci.2017.5.709

Krause-Jensen, D., C. M. Duarte, I. E. Hendriks, L. Meire, M. E. Blicher, N. Marbà, and M. K. Sejr. 2015. Macroalgae contribute to nested mosaics of pH variability in a subarctic fjord. Biogeosciences **12**: 4895–4911. doi:10.5194/bg-12-4895-2015

Lees, D. C., J. P. Houghton, D. E. Erikson, W. B. Driskell, and D. E. Boettcher. 1980. Ecological studies of intertidal and shallow subtidal habitats in Lower Cook Inlet, AK. Final Report to NOAA OSCSEAP.

Lowe, A. T., J. Bos, and J. Ruesink. 2019. Ecosystem metabolism drives pH variability and modulates long-term ocean acidification in the Northeast Pacific coastal ocean. Sci. Rep. **9**: 963. doi:10.1038/s41598-018-37764-4

Lueker, T. J., A. G. Dickson, and C. D. Keeling. 2000. Ocean pCO_2 calculated from dissolved inorganic carbon, alkalinity, and equations for K_1 and K_2: Validation based on laboratory measurements of CO_2 in gas and seawater at equilibrium. Mar. Chem. **70**: 105–119. doi:10.1016/S0304-4203(00)00022-0

Martz, T. R., J. G. Connery, and K. S. Johnson. 2010. Testing the Honeywell Durafet® for seawater pH applications. Limnol. Oceanogr.: Methods **8**: 172–184. doi:10.4319/lom.2010.8.172

Mathis, J. T., and R. A. Feely. 2013. Building an integrated coastal ocean acidification monitoring network in the U.S. Elem. Sci. Anthr. **1**: 000007. doi:10.12952/journal.elementa.000007

Mathis, J. T., and others. 2015*a*. Ocean acidification risk assessment for Alaska's fishery sector. Prog. Oceanogr. **136**: 71–91. doi:10.1016/j.pocean.2014.07.001

Mathis, J. T., J. N. Cross, W. Evans, and S. C. Doney. 2015*b*. Ocean acidification in the surface waters of the Pacific-Arctic boundary regions. Oceanography **28**: 122–135. doi:10.5670/oceanog.2015.36

McCutcheon, M. R., C. J. Staryk, and X. Hu. 2019. Characteristics of the carbonate system in a semiarid estuary that experiences summertime hypoxia. Estuaries Coasts **42**: 1509–1523. doi:10.1007/s12237-019-00588-0

Miller, R. J., D. C. Reed, and M. A. Brzezinski. 2011. Partitioning of primary production among giant kelp (*Macrocystis pyrifera*), understory macroalgae, and phytoplankton on a temperate reef. Limnol. Oceanogr. **56**: 119–132. doi:10.4319/lo.2011.56.1.0119

Miller, C. A., K. Pocock, W. Evans, and A. L. Kelley. 2018. An evaluation of the performance of sea-bird Scientific's autonomous SeaFET™: Considerations for the broader oceanographic community. Ocean Sci. **2018**: 1–32. doi:10.5194/os-2018-52

Newton, J., R. Feely, E. Jewett, P. Williamson, and J. Mathis. 2015. Global ocean acidification observing network: Requirements and governance plan, 2nd ed. Ocean Acidification International Coordination Centre of the IAEA.

Orr, J. C., J.-M. Epitalon, A. G. Dickson, and J. P. Gattuso. 2018. Routine uncertainty propagation for the marine carbon dioxide system. Mar. Chem. **207**: 84–107. doi:10.1016/j.marchem.2018.10.006

Pacella, S. R., C. A. Brown, G. G. Waldbusser, R. G. Labiosa, and B. Hales. 2018. Seagrass habitat metabolism increases short-term extremes and long-term offset of CO_2 under future ocean acidification. Proc. Natl. Acad. Sci. USA **115**: 3870–3875. doi:10.1073/pnas.1703445115

Pilcher, D. J., D. M. Naiman, J. N. Cross, A. J. Hermann, S. A. Siedlecki, G. A. Gibson, and J. T. Mathis. 2019. Modeled effect of coastal biogeochemical processes, climate variability, and ocean acidification on aragonite saturation state in the Bering Sea. Front. Mar. Sci. **5**. doi:10.3389/fmars.2018.00508

Reisdorph, S. C., and J. T. Mathis. 2015. Assessing net community production in a glaciated Alaskan fjord. Biogeosciences **12**: 5185–5198. doi:10.5194/bg-12-5185-2015

Schoch, G. C., and H. Chenelot. 2004. The role of estuarine hydrodynamics in the distribution of kelp forests in Kachemak Bay, Alaska. J. Coast. Res. **2009**: 179–195. doi:10.2112/SI45-179.1

Siedlecki, S. A., D. J. Pilcher, A. J. Hermann, K. Coyle, and J. Mathis. 2017. The importance of freshwater to spatial variability of aragonite saturation state in the Gulf of Alaska. J. Geophys. Res. Oceans **122**: 8482–8502. doi:10.1002/2017JC012791

Strom, S. L., M. B. Olson, E. L. Macri, and C. W. Mordy. 2006. Cross-shelf gradients in phytoplankton community structure, nutrient utilization, and growth rate in the coastal Gulf of Alaska. Mar. Ecol. Prog. Ser. **328**: 75–92. doi:10.3354/meps328075

Trasky, L. L., L. B. Flagg, and D. C. Burbank. 1977. Impact of oil on the Kachemak Bay environment, Environmental studies of Kachemak Bay and lower Cook Inlet. **1**: Alaska Dept. of Fish and Game, Marine Coastal Habitat Management.

Uppström, L. R. 1974. The boron/chlorinity ratio of deep-sea water from the Pacific Ocean. Deep-Sea Res. Oceanogr. Abstr. **21**: 161–162. doi:10.1016/0011-7471(74)90074-6

Van Dam, B. R., and H. Wang. 2019. Decadal-scale acidification trends in adjacent North Carolina estuaries: Competing role of anthropogenic CO_2 and riverine alkalinity loads. Front. Mar. Sci. **6**. doi:10.3389/fmars.2019.00136

Van Heuven, S., D. Pierrot, J. W. B. Rae, E. Lewis, and D. W. R. Wallace. 2011. MATLAB program developed for CO_2 system calculations. https://doi.org/10.3334/CDIAC/otg.CO2SYS_MATLAB_v1.1

Waldbusser, G. G., and J. E. Salisbury. 2014. Ocean acidification in the coastal zone from an organism's perspective: Multiple system parameters, frequency domains, and habitats, p. 221–247.*In* C. A. Carlson and S. J. Giovannoni [eds.], Annual review of marine science, v. **6**. Annual Reviews.

Waldbusser, G. G., B. Hales, C. J. Langdon, B. A. Haley, P. Schrader, E. L. Brunner, M. W. Gray, C. A. Miller, and I. Gimenez. 2015. Saturation-state sensitivity of marine bivalve larvae to ocean acidification. Nat. Clim. Change **5**: 273–280. doi:10.1038/NCLIMATE2479

Wallace, R. B., and C. J. Gobler. 2015. Factors controlling blooms of microalgae and macroalgae (*Ulva rigida*) in a eutrophic, urban estuary: Jamaica Bay, NY, USA. Estuaries Coasts **38**: 519–533. doi:10.1007/s12237-014-9818-1

Wanninkhof, R. 2014. Relationship between wind speed and gas exchange over the ocean revisited. Limnol. Oceanogr.: Methods **12**: 351–362. doi:10.4319/lom.2014.12.351

Welch, P. 1967. The use of fast Fourier transform for the estimation of power spectra: A method based on time averaging over short, modified periodograms. IEEE Trans. Audio Electroacoust. **15**: 70–73. doi:10.1109/TAU.1967.1161901

Welschmeyer, N. A., S. Strom, R. Goericke, G. DiTullio, M. Belvin, and W. Petersen. 1993. Primary production in the subarctic Pacific Ocean: Project SUPER. Prog. Oceanogr. **32**: 101–135. doi:10.1016/0079-6611(93)90010-B

Xue, L., W.-J. Cai, T. Takahashi, L. Gao, R. Wanninkhof, M. Wei, K. Li, L. Feng, and W. Yu. 2018. Climatic modulation of surface acidification rates through summertime wind forcing in the Southern Ocean. Nat. Commun. **9**: 3240. doi:10.1038/s41467-018-05443-7

Acknowledgments

The authors would like to thank Hans Pedersen, Mike Geagel, and Kris Holderied from the NOAA Kasitsna Bay Laboratory, Seldovia, AK, U.S.A. All data used in this manuscript are either presented in Table S2 or will be made available at (https://www.dataone.org/). Funding support: BOEM award No. M17AC00011 to A.L.K.

Conflict of Interest

None declared.

Submitted 16 October 2019
Revised 10 April 2020
Accepted 18 December 2020

Editor-in-Chief: K. David Hambright